Karlsruher Institut für Technologie

FE-Study on heart-shaped crack-tip zones

G. Rizzi, K.G. Schell, C. Bucharsky, T. Fett

KIT SCIENTIFIC WORKING PAPERS 142

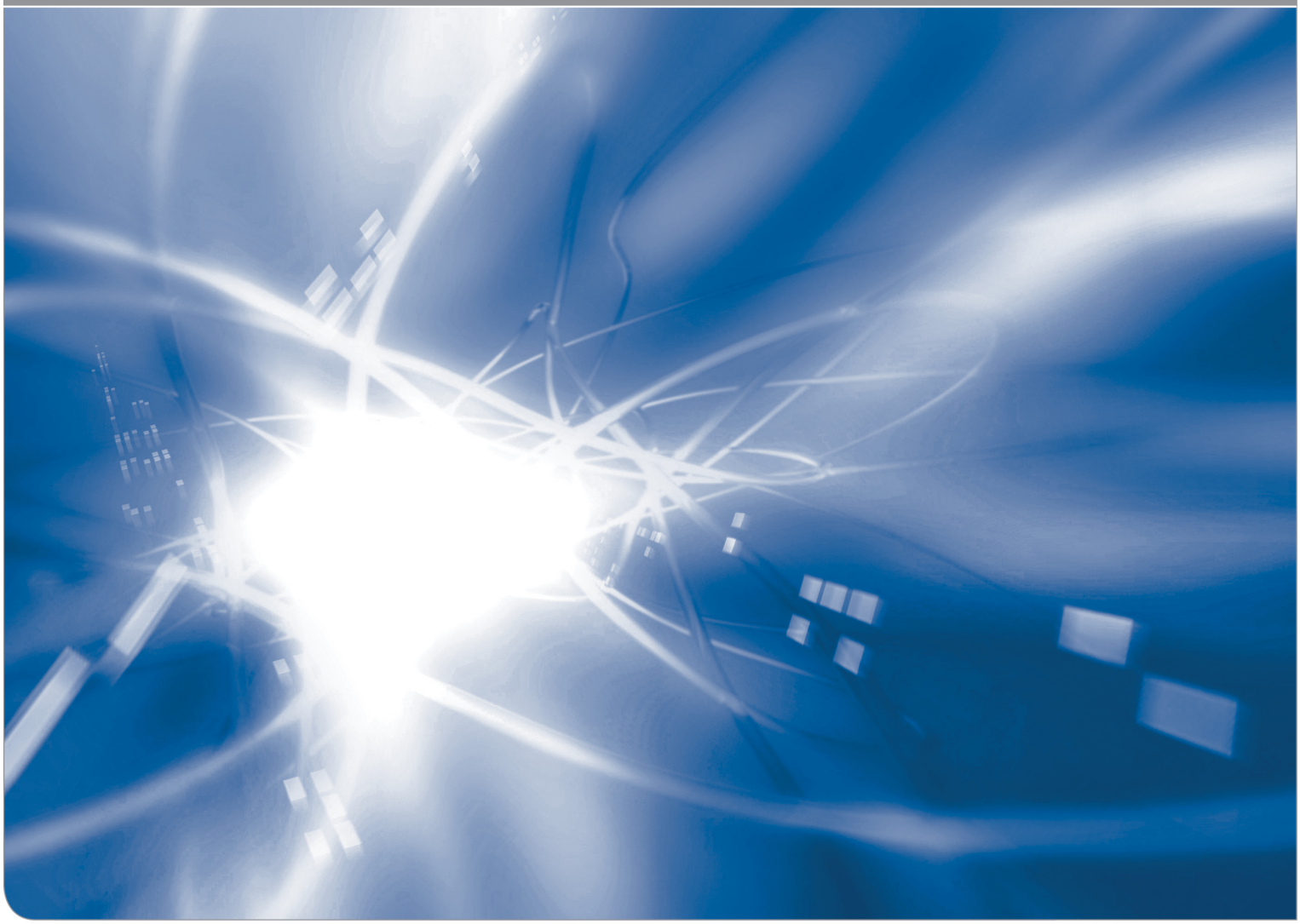

KIT – Universität des Landes Baden-Württemberg und nationales Forschungszentrum in der Helmholtz-Gemeinschaft

IAM Institute for Applied Materials

Impressum

Karlsruher Institut für Technologie (KIT)
www.kit.edu

2020

ISSN: 2194-1629

Abstract

When water penetrates into silica surfaces near a crack tip, it reacts with the SiO_2 network and generates hydroxyl ≡SiOH. Due to the hydroxyl generation, the originally intact SiO_2 rings are damaged and the structure becomes more compliant. One consequence is a reduced Young's module in the damaged zone.

In this report the general influence of different moduli ahead of a crack tip and in the bulk on the stress intensity factors will be studied by Finite Element modeling.

From the FE results it can be concluded that within the numerical errors

a) the J-integral gives the same results as the evaluation of stresses and crack openings, and

b) the crack-tip stress intensity is proportional to the externally applied one and to the square root of the Young's modulus at the crack tip.

The slender notch is considered as an example of application.

Contents

1. Introduction

The reaction of water and silica in the surface diffusion zone affects the fracture mechanics stress intensity factor K at the tips of cracks. At temperatures $T < 450°C$, the equilibrium constant of the water/silica-reaction

$$\equiv\text{Si-O-Si}\equiv + H_2O \leftrightarrow \equiv\text{SiOH+HOSi}\equiv \tag{1}$$

is given by

$$k_1 = \frac{S}{C}. \tag{2}$$

where, $S = [\equiv\text{SiOH}]$, is the concentration of the hydroxyl groups in the silica network and $C = [H_2O]$ the concentration of unreacted water.

According to Le Chatelier [1], the equation governing the equilibrium constant is

$$\frac{\partial \ln k_1}{\partial p} = -\frac{\Delta\overline{V}}{RT}. \tag{3}$$

where p is pressure, $\Delta\overline{V}$ is the reaction volume, R the universal gas constant, and T the temperature in °K.

In gases and liquids, the loading is always hydrostatic. In a solid the situation is more complicated, since the individual stress components σ_x, σ_y, σ_z are in general independent of each other and are not necessarily hydrostatic. Especially in uniaxial tension or compression, the hydrostatic stress deviates clearly from the tensile stress. In contrast to this, the stress state ahead of crack tips is more hydrostatic since the stress in the prospective plane and the stress normal on this plane are identical, $\sigma_x=\sigma_y$, and the stress σ_z is very close to the tip: $\sigma_z=\nu(\sigma_x+\sigma_y)$.

By replacing the hydrostatic pressure p by the hydrostatic stress σ_h in a solid

$$\sigma_h = \tfrac{1}{3}(\sigma_x + \sigma_y + \sigma_z) \tag{4}$$

we obtain with the hydroxyl concentration S_0 for $\sigma_h=0$

$$S = S_0 \exp\left(\frac{\sigma_h \Delta\overline{V}}{RT}\right) \quad , \quad \sigma_h = -p \tag{5}$$

For a crack of depth a, the singular hydrostatic near-tip stresses are given as

$$\sigma_h = \tfrac{2}{3}(1+\nu)\frac{K}{\sqrt{2\pi r}}\cos(\varphi/2) \tag{6}$$

where r and φ are the polar coordinates with the origin at the crack tip, see Fig. 1a. Equations (5) and (6) imply that in the high crack-tip stress field nearly all water is present in form of hydroxyl S.

The shape $r(\varphi)$ of the zone contour for constant σ_h in plane strain results from eq.(6) as

$$r = \frac{8}{3\sqrt{3}} \omega \cos^2(\theta/2) \tag{7}$$

with the height ω of the zone for a prescribed hydrostatic stress

$$\omega = \frac{(1+\nu)^2}{4\sqrt{3}\pi} \left(\frac{K_I}{\sigma_h} \right)^2 \tag{8}$$

The contour of constant hydrostatic stress according to eqs.(7, 8) is shown in Fig. 1a as the heart-shaped curve. This contour also describes the damage zone in front of the tip of a crack that has not yet grown by subcritical or stable crack growth.

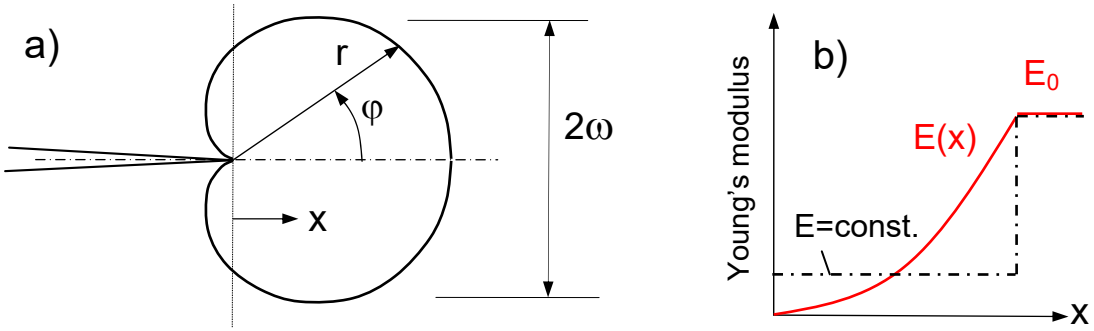

Fig. 1 a) Contour for a constant hydrostatic stress ahead of a loaded crack, b) variation of Young's modulus in a frontal zone $E(x)$ (red curve), replaced by an average constant modulus E.

The hydroxyl generation by the reaction (1) causes damage since the originally intact silica ring structure is cracked by the water attack. One of the consequences of such damage is the reduction of Young's modulus E.

When E_D is the modulus in the damaged state and E_0 the value for undamaged silica, we could derive the relation [2]

$$\frac{E_D}{E_0} = (1 - \gamma S)^2 = (1 - S/S_{max})^2 \tag{9}$$

with γ=5.3 [4.35, 6.25] (90%-CI in brackets) and the hydroxyl concentration at which the Young's modulus disappears $S_{max} = 1/\gamma = 0.188$ [0.16, 0.23].

As Fig. 1a shows, the tip of the crack is not embedded in the heart-shaped zone but terminates at r=0. This point in principle belongs to both the frontal zone and the undamaged surrounding material. A description by eq.(9) leads to a variable module distribution $E(x)$, which is replaced here by an average constant value for reasons of simplicity, Fig. 1b. The module E_0 prevails outside the crack-tip zone.

Another reason for the decrease in the elasticity module in the "frontal process zone" is microcracking in polycrystalline ceramics as was studied by Evans and Faber [3].

2 Crack terminating at φ=π of the heart-shaped zone

2.1 Constant modulus over the zone size

First we studied the case that a constant modulus is prescribed over the whole zone. In the heart-shaped zone the Young's modulus is $E \leq E_0$ and outside the zone E_0. FE calculations were performed with ABAQUS 6.9 and 6.12. For simplicity, ω=1, σ_{appl}=1, and E_0=1 were chosen. Table 1 shows the J-integrals according to Rice [4] and the stress intensity factors obtained from the first contours for the lowest Young's modulus of E=0.01 E_0. Apart from the first contour, the results are almost constant. Due to symmetry, no mode-II stress intensity factor could appear. The average mode-I stress intensity factor over contour 2-8 is 1.974 and the Standard Deviation 0.00125 (0.06%).

Contour	J	K_I	K_{II}
1	370.3	1.953	0
2	378.0	1.973	0
3	378.0	1.973	0
4	378.1	1.973	0
5	378.6	1.975	0
6	379.2	1.976	0
7	379.6	1.977	0
8	378.8	1.975	0

Table 1 J-integral and stress intensity factors for the first contours (E/E_0=0.01, E_0=1, ν=0.17, ω=1).

The interrelation between crack opening displacement v and stress intensity factor K_I is for the near-tip field along the symmetry line (here: $-x=r<<\omega$) in plain strain with $E'=E_0/(1-\nu^2)$

$$K_I = \sqrt{\frac{\pi}{8}} v \frac{E'}{\sqrt{r}} \tag{10}$$

Normalized displacements v' represented in Fig. 2 are defined as

$$v' = v \frac{E_0}{\sigma_{appl}\,\omega(1-\nu^2)} \tag{10a}$$

The stress intensity factors obtained from the least-squares fit of displacements in Fig. 2 are compiled in Table 2, Column 3.

An independent procedure for the stress intensity factor determination is the evaluation of the near-tip stresses ahead of the crack tip, i.e. the stresses along the prospective crack propagation plane. For the normal component on this plane it holds for the first terms

$$\sigma_{yy} = \frac{K}{\sqrt{2\pi x}} + A\sqrt{x} \tag{11}$$

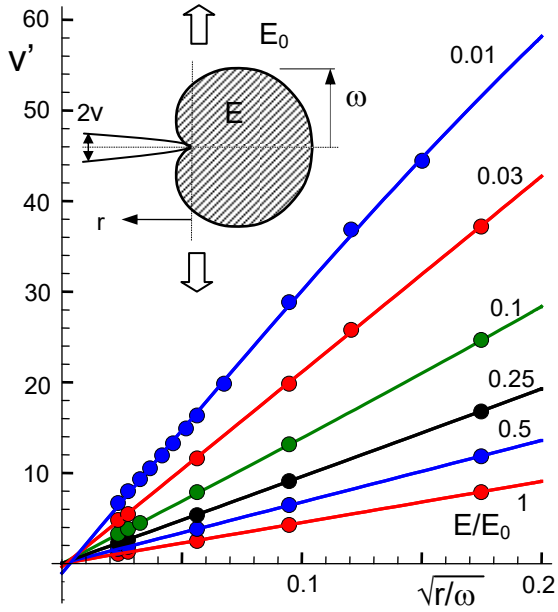

Fig. 2 FE-results of near-tip CODs fitted according to eq.(10).

A regression analysis of the data in Fig. 3 provides the stress intensity factors. The results obtained from the data fit of Fig. 3 are compiled in Table 2, Column 4 in the dimensionless form of

$$K' = \frac{K}{\sigma_{appl}\sqrt{\omega}} \tag{11a}$$

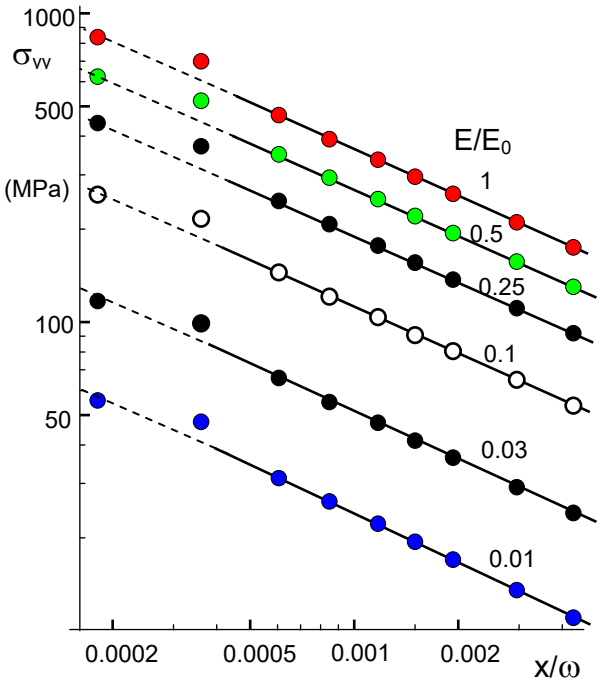

Fig. 3 Stress σ_{yy} along the prospective crack propagation line (φ=0), lines: fitting curves according to eq.(11), yielding the stress intensity factor for the data points in the range of $0.0005<x/\omega<0.004$.

2.2 Step-shaped modulus distribution

So far only cases with a constant modulus were studied, Fig. 4a. An additional FE-evaluation was made for the case of a variable modulus in the zone ahead the tip. As Fig. 4 shows, the modulus was varied in 4 steps. In the inner zone of Fig. 4b, the modulus E was E=0.25 E_0, then E=0.57 E_0, E=0.72 E_0, and outside E=E_0. The result from the J-Integral was (for E_0=1, ν=0.17, σ_{appl}=1 and ω=1): K'=14.83, hardly different from the case of constant modulus E=0.25 E_0. Also this value is introduced in the second Column of Table 2.

	K', eq.(11a)		
E/E_0	via J	via COD	via σ_{yy}
1	29.21	29.11	28.78
0.5	21.82	21.81	21.58
0.25	15.43	15.40	15.21
0.25/0.57/0.72/1.	14.83	-	-
0.1	9.039	8.871	8.892
0.03	4.141	4.153	4.065
0.01	1.974	1.997	1.943

Table 2 Normalized stress intensity factors K' from J-Integral, COD, and near-tip stress σ_{yy} in the form of eq.(11a).

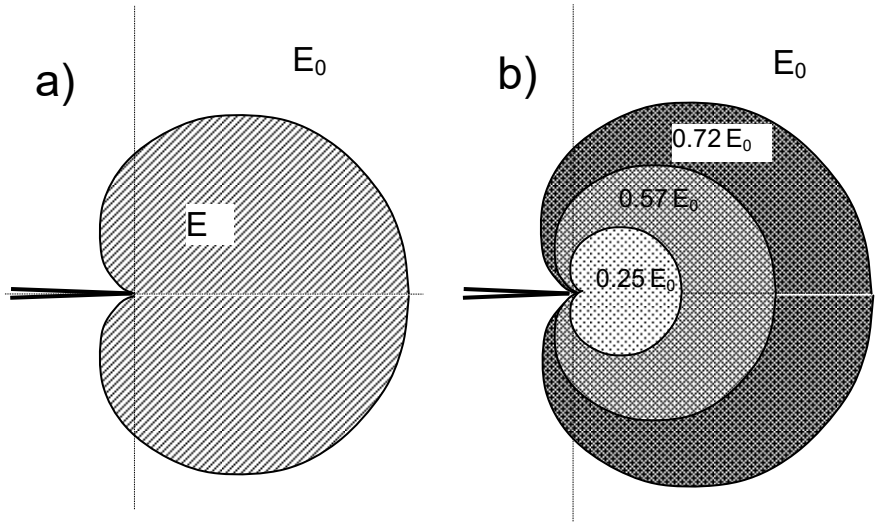

Fig. 4 a) Crack-tip zone with a Young's modulus E deviating from the bulk modulus E_0, E<E_0, b) stepwise decreasing modulus in zones of height 1/3, 2/3, and 3/3ω.

The K-values for the single zones of Fig. 4a, compiled in Table 2, are plotted in Fig. 5a by the symbols (for the geometric data see the insert). In this plot the stress intensity factors were normalized on the J-based K value at E/E_0=1. The triangle corresponds to the varying Young's modulus shown in Fig. 4b.

Figure 5b represents the ratio of the data for COD- and σ_{yy}-based stress intensity factors normalized on the stress intensity factors from the J-Integral. The hatched area indicates the region of data scatter with an average and "scatter" of about

$$K(E)/K_J(E) \cong 0.993 \pm 0.015$$

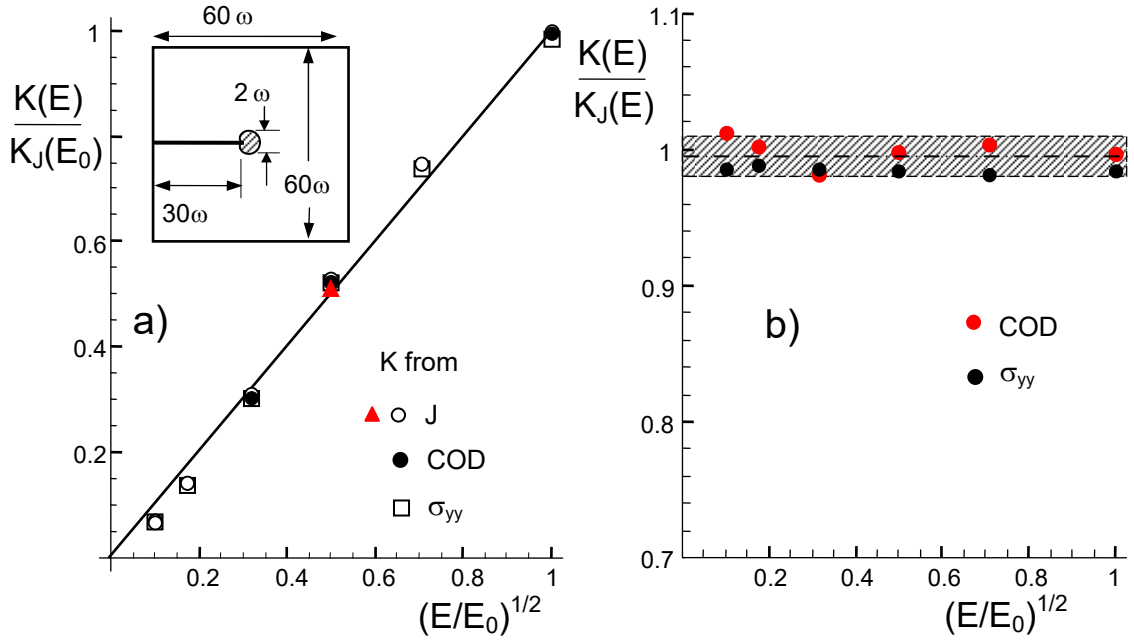

Fig. 5 a) Stress intensity factors from J-Integral, COD, and near-tip stress σ_{yy}, (K-values normalized on the result from J-Integral for E/E_0=1), red triangle for step-shaped E-distribution, b) comparison of K from COD and σ_{yy} with the individual results from J-Integral

2.3 Conclusions from the FE-analysis

From the results of Fig. 5 it becomes evident that

- the stress intensity factors are roughly independent of the computation method,
- the stress intensity factor is only affected by the modulus closest to the crack tip,
- the straight-line behaviour of Fig. 5a suggests the representation by

$$K \cong K_{appl}\sqrt{\frac{E}{E_0}} \tag{12}$$

The FE results confirm eq.(12) as had to be expected e.g. from the theoretical analysis by Merkle [5] on slender notches embedded in the reduced modulus at the notch-root. From the agreement between the theoretical solution by Merkle [5] and the FE-results for $0.1 \leq E/E_0 \leq 1$, it can be concluded that our crack-zone modelling and the accuracy of our FE-mesh is sufficient at least for this range. For the lowest value of $E/E_0 \leq 0.01$, the FE-program indicated convergence problems.

3. Example of application: Slender notch approach of cracks

3.1 Notch-model and stresses

In a micro-structurally motivated approach, the crack tip region (Fig. 6a) is considered as a slender notch with root radius ρ in the order of the average radius of the SiO_2 rings, Fig. 6b. This description may be applied in the following considerations. For such a notch, Wiederhorn et al. [6] suggest a crack-tip radius of ρ = 0.5 nm.

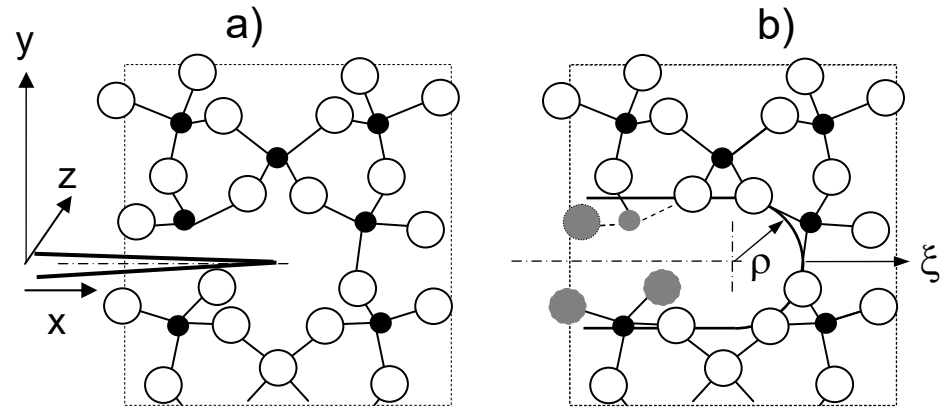

Fig. 6 a) Crack in silica terminating in a nano-pore, b) equivalent slender notch with a finite notch root radius ρ, grey molecules are mechanically inactive.

Stresses at slender notches were given by Creager and Paris [7]. The stress component normal to the crack plane (the tangential stress $\sigma_t=\sigma_y$) is at the notch root

$$\sigma_y = \frac{2K}{\sqrt{\pi \rho}} \tag{13}$$

The other stress components are

$$\sigma_x = 0 \tag{14}$$

$$\sigma_z = \frac{2\nu K}{\sqrt{\pi \rho}} \tag{15}$$

Consequently, the hydrostatic stress term results as

$$\sigma_h = \frac{2(1+\nu)K}{3\sqrt{\pi\rho}} \tag{16}$$

Equation (16) makes clear that the stresses in realistic silica structures remain finite whatever the applied stress intensity factor is. On the other hand, Merkle [5] had shown that relation (12) also holds for notches.
These two findings make clear that always: $E/E_0>0$ and, consequently, $K>0$.

3.2 Applicability of J-Integral to hydroxyl damage

It has been shown in many papers that the J-Integral is applicable to sharp-crack problems when the crack-tip damage shows a saturation value. This was for instance shown for micro crack damage in polycrystalline ceramics by Evans and Faber [3]. In the following considerations the damage by hydroxyl generation will be addressed.
Using eqs.(5),(9), and (12) a simple approximation for the stress intensity factor in the damaged region is obtained as:

$$K_D \cong K_{appl}(1-\tfrac{1}{2}\lambda S) \tag{17}$$

Next, we will compute the local hydroxyl concentration and the damage as a function of the externally applied stress intensity factor K_{appl}.
Crack extension under inert conditions occurs when the maximum stress at the notch equals fracture toughness K_{Ic}. Then the tangential component σ_y at the notch root reaches a critical stress value σ_0:

$$\frac{2K_{Ic}}{\sqrt{\pi\rho}} = \sigma_0 \tag{18}$$

The related hydrostatic stress at fracture is

$$\sigma_{h,0} = \frac{(1+\nu)K_{appl}}{3K_{Ic}}\sigma_0 \tag{19}$$

The critical stress can be interpreted as the ideal or theoretical strength σ_0. Its value is about [8]

$$\sigma_0 = \frac{E}{\pi} \cong 23\,\text{GPa} \tag{20}$$

as is in agreement with strengths up to 25 GPa measured by Brambilla and Payne [9] on extremely thin silica fibers of about 60 nm radius. The highest tensile strengths for thicker silica glass fibers in ultra-high vacuum are about $\sigma_c \cong 12.6$ GPa [10] at room temperature.
From eqs.(5) and (19) it follows for the damaged material

$$S = S_0 \exp\left[\gamma \frac{K_D}{K_{\mathrm{Ic}}} \right], \quad \gamma = \tfrac{1}{3}(1+\nu)\frac{\sigma_0 \Delta \overline{V}}{RT} \tag{21}$$

and with eq.(17),

$$S = S_0 \exp\left[\gamma \frac{K_{appl}}{K_{\mathrm{Ic}}} (1 - \tfrac{1}{2}\lambda\, S) \right] \tag{22}$$

The unknown quantity S appears on both sides of (22). This implicit equation in S is solved by

$$S = S_{\max} \frac{K_{\mathrm{Ic}}}{\gamma K_{appl}} \mathrm{PLog}\left[\gamma \frac{K_{appl}}{S_{\max} K_{\mathrm{Ic}}} S_0 \exp\left(\gamma \frac{K_{appl}}{K_{\mathrm{Ic}}} \right) \right] \tag{23}$$

where the "PLog" stands for the Lambert W function or *product log function*, i.e. the solution W=PLog(z) of the equation z=W exp(W) [11].
Due to eq.(17) a similar relation holds for the notch-root stress intensity factor

$$K_D = K_{appl}\left(1 - \frac{K_{\mathrm{Ic}}}{\gamma K_{appl}} \mathrm{PLog}\left[\gamma \frac{K_{appl}}{S_{\max} K_{\mathrm{Ic}}} S_0 \exp\left(\gamma \frac{K_{appl}}{K_{\mathrm{Ic}}} \right) \right] \right) \tag{24}$$

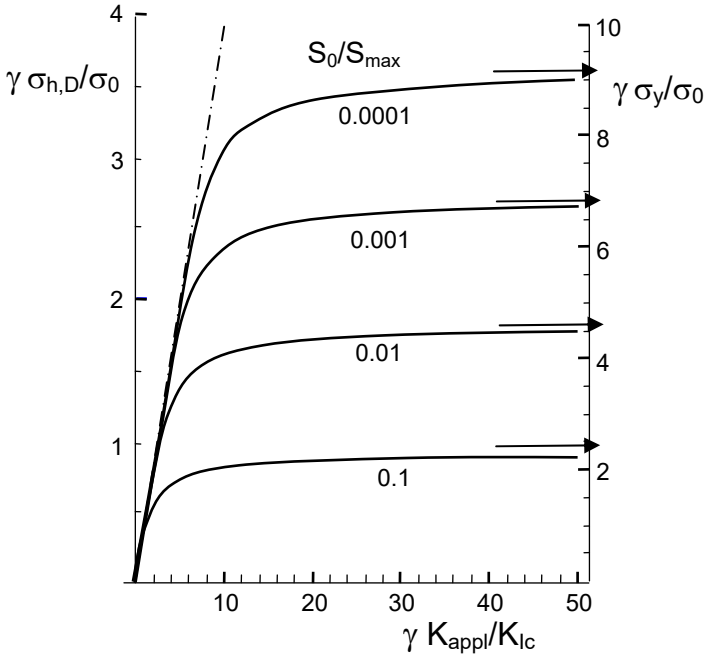

Fig. 7 Hydrostatic stress in the hydroxyl-damaged state, $\sigma_{h,D}$, normalized on the critical stress (ideal strength) σ_0 as a function of the applied stress intensity factor K_{appl} (normalized representation), right ordinate: tangential stress $\sigma_{t,D}$=$\sigma_{y,D}$ at the notch root normalized on critical strength σ_0.

The hydrostatic stress under damage conditions

$$\sigma_{h,D} = \frac{(1+\nu)K_D}{3K_{Ic}}\sigma_0 \quad , \quad \gamma = \tfrac{1}{3}(1+\nu)\frac{\sigma_0 \Delta \overline{V}}{RT} \tag{25}$$

is plotted in Fig. 7 as a function of the remote stress intensity factor K_{appl} and the hydroxyl concentration S_0 at the notch root before load application.

The maximum possible hydrostatic stress reads

$$\sigma_{h,D,\max} = -\frac{1}{\gamma}\text{Log}\left[\frac{S_0}{S_{\max}}\right] \tag{26}$$

The limit values from (26) are represented by the arrows in Fig. 7.

Figure 8 illustrates the typical stress vs. strain curve for a material damaged by micro cracking reaching saturation damage (black curve) and hydroxyl damaged silica (red curve) with its nearly flat stress-strain curve. It should be noted that this type of curve holds also for the tangential stress component since $\sigma_y = 3\sigma_h/(1+\nu)$.

Since the maximum stress at the notch root is finite (circle in Fig. 8) for certain prescribed K_{appl}, it does not matter what the further part of the material curve looks like. Two possible curve extensions are given by (A) and (B), both of them must lead to the same result.

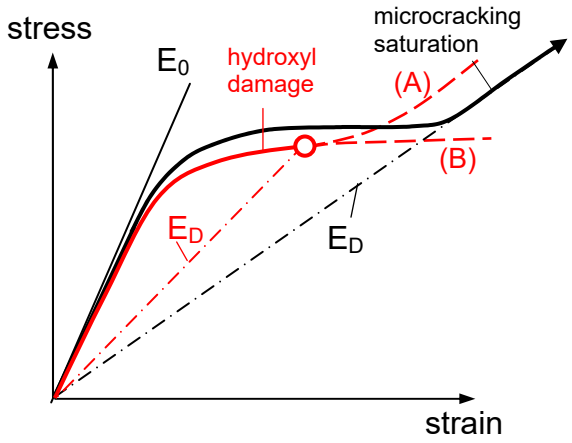

Fig. 8 Stress vs strain curves for a polycrystalline ceramic showing microcracking (black, solid curve) and silica (red, solid curve) showing hydroxyl damage. Maximum stress at a notch root indicated by the circle, hypothetical extension of the material curve under hydroxyl damage denoted as (A) and (B).

References

1 H. Le Chatelier, *C.R. Acad. Sci. Paris* **99**(1884), 786.

2 T. Fett, G. Schell, C. Bucharsky, Hydroxyl Damage in Silica: Full-range description including large damages **126**, 2019, ISSN: 2194-1629, Karlsruhe, KIT.

3 Evans, A.G., Faber, K.T., Crack-growth resistance of microcracking brittle materials, J. Am. Ceram. Soc. **67**(1984), 255-260.

4 Rice, J.R., A path independent integral and the approximate analysis of strain concentration by notches and cracks, Trans. ASME, J. Appl. Mech. (1986), 379-386.

5 J. G. Merkle, An application of the J-integral to an incremental analysis of blunt crack behavior, Mechanical Engineering. Publications, London, 1991, 319-332.

6 S.M. Wiederhorn, E.R. Fuller, Jr. and R. Thomson, "Micromechanisms of crack growth in ceramics and glasses in corrosive environments," Metal Science, **14**(1980), 450-8.

7 Creager, M., Paris, P.C., Elastic field equations for blunt cracks with reference to stress corrosion cracking, Int. J. Fract. **3**(1967), 247-252.

8 Silva, E. C. C. M.; Tong, L.; Yip, S.; Van Vliet, K. J. *Small* **2005**, *2*, 239–243.

9 G. Brambilla, D.N. Payne, The ultimate strength of glass silica nanowires, Nano Letters, **9**(2009), 831-835.

10 C.R. Kurkjian, P.K. Gupta, R.K. Brow, and N. Lower, "The intrinsic strength and fatigue of oxide glasses," *J. Noncrystal. Solids*, **316** 114-124 (2003)

11 R. Corless, G. Gonnet, D. Hare, D. Jeffrey and D. Knuth, "On the Lambert W Function," Advances in Computational Mathematics, **5**(1996), 329-359.

KIT Scientific Working Papers
ISSN 2194-1629

www.kit.edu